Fuel 259 (2020) 116228

Contents lists available at ScienceDirect

Fuel

journal homepage: www.elsevier.com/locate/fuel

Full Length Article

Detailed chemical kinetic modeling of fuel-rich n-heptane flame

Emre Degirmenci, Abdalwahab Alazreg, Fikret Inal*

Department of Chemical Engineering, Izmir Institute of Technology, Gulbahce-Urla, 35430 Izmir, Turkey

ARTICLE INFO

Keywords:
n-Heptane
Detailed chemical kinetic modeling
Premixed flame
PAH

ABSTRACT

The main purpose of this study is to model one-dimensional, premixed, laminar, burner-stabilized, fuel-rich n-heptane flame to understand its combustion characteristics. Detailed chemical kinetic modeling technique was used to obtain more information about the formation nature of emissions in n-heptane flame. A detailed chemical kinetic mechanism was generated by combining several mechanisms from the literature that related with possible products of fuel-rich n-heptane combustion. The mechanism consists of 4185 reactions and 893 species. Validations of the mechanism were done by species mole fractions of premixed laminar flames and jet stirred reactors, and ignition delay times in shock tubes. A detailed investigation of the n-heptane flame was carried out using rate of production and reaction pathway analyses. Propargyl radical (C_3H_3), vinylacetylene (C_4H_4) and acetylene (C_2H_2) were found as the main precursors of benzene formation. The mechanism was able to predict most of the major, minor, and trace species up to four-fused aromatic rings formed in the flame. A skeletal mechanism was also generated using Directed Relation Graph with Error Propagation (DRGEP) method. It consists of 1879 reactions and 359 species. The skeletal mechanism was in a good agreement with the detailed mechanism on the species mole fraction predictions.

1. Introduction

Most of the utilized energy in the world comes from numerous combustion-related sources. Combustion has a variety of application areas such as power generation, transportation, and industrial manufacturing operations. On the other side, combustion is one of the major sources of environmental pollutants. The incomplete combustion of the hydrocarbon fuel is the main reason behind polycyclic aromatic hydrocarbon (PAH) formation. PAHs consist of two or more aromatic rings that are bonded with linear, angular or cluster form in their structures. They are toxic and carcinogenic compounds [1]. PAHs can be formed from a combination of simpler aromatic rings such as benzene (C_6H_6) or they can also be formed as an aromatic compound from non-aromatic species [2]. The high-molecular-weight PAHs (500–1000 amu) are considered as precursors of soot particles [3]. n-Heptane is a component of commercial gasoline and one of the primary reference fuels (PRF) for the determination of gasoline octane number.

The oxidation of n-heptane has been studied extensively in the literature. Bakali et al. [4] have investigated the oxidation of a laminar premixed n-Heptane/O_2/N_2 flame experimentally with an equivalence ratio of 1.9. Species concentration profiles for intermediates, major and minor products up to benzene were measured over the flame using microprobe and online GC/MS system.

Doute et al. [5] have studied chemical structures of low-pressure, premixed n-Heptane/O_2/Ar and *iso*-Octane/O_2/Ar flames experimentally. Both flames have been stabilized at low pressure (6 kPa), and the measurements of species concentrations have been performed by mass spectrometric analyses of samples.

The high-temperature oxidation and pyrolysis mechanism of PRF mixtures that involves 107 species and 723 reactions was established by Chaos et al. [6]. The model showed good performance at temperatures greater than 950 K, pressures less than 15 bar, and equivalence ratio less than 2.5. Marchal et al. [7] have developed a detailed chemical kinetic mechanism that explains the formation of polycyclic aromatic hydrocarbons up to four ring structures and soot from several fuels (i.e., n-heptane, *iso*-octane, and decane).

Inal and Senkan, [8] have experimentally studied the formation of PAHs in fuel-rich n-heptane flames. The study concerned two atmospheric pressure, premixed, laminar n-heptane flames with equivalence ratios of 1.97 and 2.10. Using online GC/MS analyses of the samples withdrawn from the flames, species mole fraction profiles up to four aromatic rings with respect to height above the burner surface (HAB) were obtained.

A detailed kinetic mechanism of n-heptane that consists of 1400 reactions and 350 species for the growth pathways of large PAHs was developed by Raj et al. [9]. Alternative formation pathways for

* Corresponding author.
E-mail address: fikretinal@iyte.edu.tr (F. Inal).

https://doi.org/10.1016/j.fuel.2019.116228
Received 15 April 2019; Received in revised form 5 August 2019; Accepted 17 September 2019
Available online 27 September 2019
0016-2361/

Nomenclature

DCKM	Detailed Chemical Kinetic Modeling
DRG	Directed Relation Graph Method
DRGEP	Directed Relation Graph with Error Propagation
DRGPFA	Directed Relation Graph Method with Path Flux Analysis
GC/MS	Gas Chromatography/Mass Spectrometry
HAB	Height Above the Burner Surface
HACA	Hydrogen Abstraction Acetylene Addition
HAMA	Hydrogen Abstraction Methyl Addition
JSR	Jet Stirred Reactor
LLNL	Lawrence Livermore National Laboratory
PAH	Polycyclic Aromatic Hydrocarbon
PRF	Primary Reference Fuels
ROP	Rate of Production Analysis
ε_j	thermocouple junction emissivity
r_{AB}	immediate error
Nu_j	Nusselt number of thermocouple junction
$v_{A,i}$	the stoichiometric coefficient of species A in the i^{th} reaction
E_a	the activation energy
ω_i	the reaction rate of the i^{th} reaction
A	pre-exponent collision frequency factor
k_{gas}	thermal conductivity of gas (W/mK)
R	universal gas constant
S	the group of all possible paths from species A to species B
T_{gas}	gas temperature (K)
T_{tj}	thermocouple junction temperature
k	reaction rate constant
β	temperature exponent
k_{g0}	assumed constant; 6.54×10^{-5} (W/mK^2)
σ	Stefan-Boltzmann constant; 5.67×10^{-8} (W/m^2K^4)
Φ	equivalence ratio

naphthalene ($C_{10}H_8$), phenanthrene ($C_{14}H_{10}$), and pyrene ($C_{16}H_{10}$) were also involved in the mechanism. The model predictions showed a good agreement with the experimental data.

A reduced chemical kinetic mechanism for gasoline reference fuel (i.e., n-heptane, *iso*-octane, and toluene) was proposed by Wang et al. [10]. The mechanism consists of 109 species and 543 reactions, which involves PAH formation kinetics. Reaction sensitivity analyses for the formation of several aromatic species were also performed. The results have shown that for benzene formation, the most effective reactions were $C_4 + C_2 \rightarrow$ Benzene and $C_3 + C_3 \rightarrow$ Benzene. For PAH formation, the most effective reaction was determined as $C_5 + C_5 \rightarrow$ Naphthalene.

Park et al. [11] have developed a detailed chemical kinetic mechanism of the gasoline surrogate fuel (i.e., n-heptane, *iso*-octane, and toluene) that describes the formation of PAH species up to coronene. The overall mechanism consists of 2021 species and 8688 reactions. Additionally, a high-temperature sub-mechanism that consists of 574 species and 3379 reactions was also proposed for premixed laminar flames and counter-flow diffusion flames. Soot formation mechanisms from pyrene (A_4) and higher PAHs species were also studied.

A low pressure (40 mbar) premixed n-heptane flame with an equivalence ratio of 1.69 was studied by Seidel et al. [12]. The concentration profiles of ~80 species up to naphthalene ($C_{10}H_8$) were determined. A detailed chemical kinetic mechanism with 349 species and 3686 reactions was generated using the experimental data of the study. The model predictions have shown acceptable performance for species concentrations, flame speed, and ignition delay time at the pressure range of 1 bar to 40 bar and at temperature range of 500 K to 2000 K.

A semi-detailed chemical kinetic mechanism that describes the formation of PAH species from toluene reference fuel was proposed by An et al. [13]. The mechanism consists of 219 species and 1229 reactions. Rate of production/consumption (ROP) analyses were done to examine the most effective reactions in benzene formation. It was observed that reaction rates of benzene formation pathway were highly dependent on temperature. For relatively low temperature range (700 K to 950 K), n-$C_4H_5 + C_2H_2 = A_1 + H$ (A_1 refers to benzene) was determined as the most important reaction. For moderate temperatures (800 K to 1400 K), the reaction C_3H_4-A + $C_3H_3 = A_1 + H$ (C_3H_4-A refers to allene/propadiene and C_3H_3 refers to propargyl) was found as an important reaction for the first aromatic ring formation. The reaction between two propargyl radicals, $C_3H_3 + C_3H_3 = A_1$, was considered as the most important reaction for high temperature (1200 K to 1530 K) benzene formation.

A detailed chemical kinetic mechanism for gasoline surrogate fuel (i.e., n-heptane, *iso*-octane, and toluene) for a wide range of engine conditions was proposed by Mehl et al. [14]. The mechanism consists of 5935 reactions and 1389 species. Validations were done with numerous experimental data for both pure fuels and various fuel blends (such as toluene/n-heptane and *iso*-octane/1-hexene). The results of the mechanism validations in JSR and shock-tubes have shown that the model was highly successful for the ignition characteristics for an equivalence ratio of 1, and the pressure and temperature ranges of 3 to 50 atm and 650 to 1200 K, respectively.

There are limited number of experimental and modeling studies in the literature reporting concentration profiles of stable low molecular weight species, aliphatics, aromatics, and polycyclic aromatic hydrocarbons for the same n-heptane flame. In this study, the main objective is to model premixed, laminar, fuel-rich, atmospheric pressure n-heptane flame at an equivalence ratio of 2.10 [8] using detailed chemical kinetic modeling technique.

2. Method

2.1. Experimental data

The experimental setup used for data acquisition has been described elsewhere [8], therefore only brief information will be presented here. A laminar, premixed, atmospheric pressure flat flame of n-Heptane/O_2/Ar was stabilized over a 50 mm diameter porous bronze burner. Argon was also used as a shield gas to protect the flame from surrounding air. The concentrations of major, minor, and trace species were established by analyzing samples withdrawn from the flame using heated quartz microprobe coupled to an online GC/MS. The experimental conditions of the flame study are given in Table 1.

2.2. Model

The Detailed Chemical Kinetic Modeling (DCKM) approach is widely used to understand the combustion processes. One of the commonly used software for DCKM is ANSYS Chemkin-Pro® [15]. In this study, a premixed, laminar, fuel-rich flame of n-heptane was modeled using ANSYS Chemkin-Pro based on the experimental work of Inal and Senkan [8].

Table 1
Inlet stream properties of the premixed n-heptane flame.

Properties	Premixed flame
Initial velocity (cm/s)	5.17
Equivalence ratio (Φ)	2.10
n-heptane (mole %)	5.50
O_2 (mole %)	28.79
Ar (mole %)	65.71

Table 2
General information of the Base, Donor, and Master Mechanisms.

Mechanisms	Number of Reactions	Number of Species	Reference
Base Mechanism	2827	627	[14]
Donor Mechanism 1	553	99	[17]
Donor Mechanism 2	672	154	[18]
Donor Mechanism 3	1110	256	[19]
Additional Reactions	74	5	[11]
Master Mechanism	**4185**	**893**	**This Study**

In order to start the modeling work, a comprehensive mechanism (i.e., Lawrence Livermore National Laboratory (LLNL) n-heptane mechanism version 3.1) [14] was selected as a Base Mechanism. The LLNL n-heptane mechanism was also validated for a wide range of conditions, and used as the base mechanism in various modeling studies [10,11,16]. The Base Mechanism does not include some important reactions for the formation of specific fuel-rich flame products such as benzene and polycyclic aromatic hydrocarbons. The Donor Mechanism 1 includes some aromatic and PAH species formation pathways with hydrogen abstraction acetylene addition (HACA) growth [17]. It was merged with the Base Mechanism. Additionally, formation pathways of linear PAH (anthracene), angular PAH (phenanthrene), and branched aromatics (indene, *cyclo*-penta[cd]pyrene, etc.) were added from the Donor Mechanism 2 [18]. The Donor Mechanism 3 includes site specific formation and oxidation pathways of benzene and PAHs up to high molecular weight species (anthracene, aceanthrylene, cyclopenta[cd]pyrene, chrysene, etc.) [19]. It was also combined with the Base Mechanism. Additional PAH and intermediate formation reactions were also added from the recent study [11]. While merging the Donor and Base Mechanisms the molecular structures of the species were taken into consideration since each mechanism has different notations to refer species. After merging these mechanisms, the resulting mechanism was called as Master Mechanism. The general information about Base, Donor, and Master Mechanisms are given in Table 2. As seen from Table 2, the number of reactions and species in the Master Mechanism were 4185 and 893, respectively. Chemkin files for the Master Mechanism can be obtained upon request from the authors.

To enhance the model predictions, some reaction rate parameters were modified with the recent kinetic data available in the literature [11,17–21] as shown in Table 3. In Table 3, the reaction rate constant is defined by the three-parameter expression,

$$k = AT^{\beta}e^{-\frac{E_a}{RT}} \quad (1)$$

where, k is the rate constant, A the pre-exponent collision frequency factor, β the temperature exponent, E_a the activation energy, T the temperature, and R the universal gas constant.

A validation work was conducted for the Master Mechanism using the experimental data from the literature. Species mole fractions obtained in jet stirred reactors [16,20] were used for mechanism validation. There were two JSRs, the first reactor (JSR1) was at 106.6 kPa, 2 s residence time, and an equivalence ratio of $\Phi = 3$ [16], and the second reactor (JSR2) was at the same conditions of JSR1 except for an equivalence ratio of $\Phi = 2$ [20]. The model predictions of Master Mechanism and experimental measurements for n-heptane, acetylene, methane and benzene mole fractions are shown in Fig. 1. The Master Mechanism slightly underestimated n-heptane mole fractions from 550 K to 700 K for both equivalence ratios but for the negative temperature coefficient region (~700 K to ~850 K) and higher temperatures, the differences between the experimental data and model predictions were smaller (Fig. 1). As seen from Fig. 1, the Master Mechanism overpredicted acetylene mole fractions by a factor of about 3 for both JSR studies, yet the formation temperature of acetylene was properly estimated (~850 K). Model predictions for benzene mole fractions were consistent with the experimental data at the equivalence ratio of 2 (Fig. 1). However, for the equivalence ratio of 3, the Master Mechanism could not predict the low temperature (550 K to 850 K) formation of benzene. Although there were over and under predictions by the Master Mechanism, generally satisfied predictions were achieved for both JSRs. Additional model validation was carried out using one dimensional, atmospheric-pressure, premixed, laminar flame data at an equivalence ratio of 1.9 [4]. Experimental mole fractions of acetylene and benzene with model predictions are given in Fig. 2. Acetylene mole fractions were predicted by the Master Mechanism with a very low error compared with the experimental data. Benzene mole fractions were underestimated by the Master Mechanism with an error less than a factor of 2. A validation work for ignition delay time was also carried out using shock-tube data at two different pressures (20 and 38 bar) with an equivalence ratio of 1 [20]. As seen from Fig. 3, for 20 bar pressure, the Master Mechanism predicted ignition delay times with a low error on a wide temperature range (726 K to 1412 K). For the pressure of 38 bar, Master Mechanism overestimated the ignition delay times by a factor of about 1.5 for temperatures from 750 K to 950 K.

In the premixed, fuel-rich n-heptane flame the temperature measurements were carried out by rapid insertion technique [8]. However, especially around the post-flame region soot deposition on the thermocouple junction was reported. The high emissivity values of soot covered thermocouple might cause heat loss from the thermocouple junction by radiation. By exerting energy balance around the thermocouple junction [22], the measured temperature profile was corrected;

$$\varepsilon_j \sigma T_{tj}^4 = \frac{k_{g0} \times Nu_j}{2d_{tc}} \times (T_{gas}^2 - T_{tj}^2) \quad (2)$$

where, d_{tc} is the thermocouple junction diameter (m), T_{gas} the gas temperature (K), k_{g0} the $\frac{k_{gas}}{T_{gas}} \equiv$ assumed constant; 6.54×10^{-5} (W/mK^2), k_{gas} the thermal conductivity of gas (W/mK), Nu_j the Nusselt number of thermocouple junction, T_{tj} the thermocouple junction temperature (K), σ the Stefan-Boltzmann constant; 5.67×10^{-8} (W/m^{2}K^4), and $\mathcal{E}_j$ the thermocouple junction emissivity.

By assuming a linear correlation between experimentally measured

Table 3
Modified rate constant parameters in the Base Mechanism.

Reactions	A (mol, cm, s units)	β	E_a (cal/mol)	Reference
H + O2 = O + OH	1.04E + 14	0	15,286	[20]
C3H5-A + H = C3H4-A + H2	5.00E + 13	0	0	[18]
C3H5-A + CH3 = C3H4-A + CH4	3.02E + 12	−0.32	−1.31E + 02	[18]
C3H4-A + CH3 = C3H3 + CH4	1.50E + 00	3.5	5.60E + 03	[18]
C3H3 + H + (M) = C3H4-P(+ M)	1.66E + 15	−0.37	0	[18]
C2H + CH3 = C3H4-P	8.00E + 46	−10	4.63E + 04	[19]
C3H3 + O = CH2O + C2H	7.17E + 13	0	0	[19]
C3H3 + OH = C3H2 + H2O	2.00E + 13	0	8.00E + 03	[11]
C3H3 + H = C3H2 + H2	2.14E + 05	2.52	7.45E + 03	[11]
C2H4 + H = C2H3 + H2	1.33E + 06	2.53	1.22E + 04	[17]
C2H3 + O2 = O + CH2 + CO	3.50E + 14	−0.611	5.26E + 03	[18]
C2H2 = H + HCCO	9.03E + 12	0	4.53E + 03	[21]

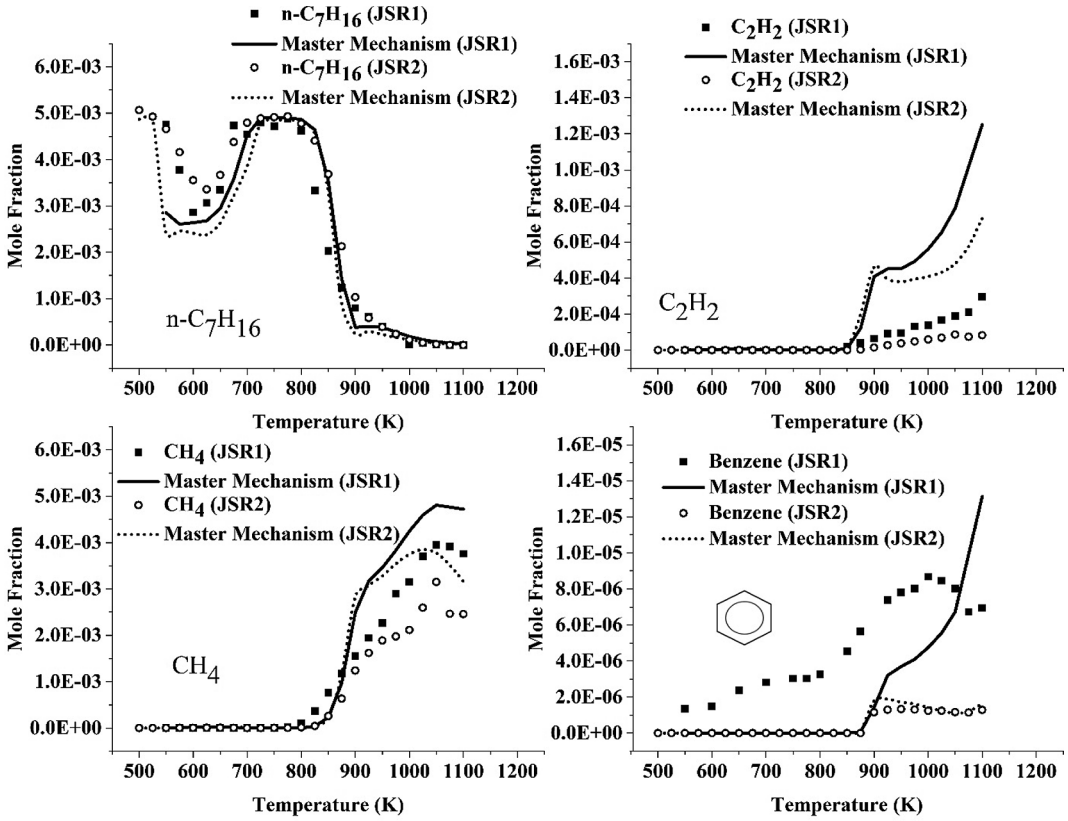

Fig. 1. Validation of the Master Mechanism for mole fractions of n-C_7H_{16}, C_2H_2, CH_4, and C_6H_6 in JSR1 (Φ = 3) [16] and JSR2 (Φ = 2) [20].

soot volume fractions and junction emissivity values, the energy balance was solved for gas temperature. As a result of the temperature corrections, the measured and corrected temperature profiles are given in Fig. 4. The radiation correction in temperature was about 70 K at 2.0 mm HAB. Similar differences between measured and corrected temperatures were also reported for premixed, fuel-rich butane (about 105 K at 1.5 mm above the burner surface) [18] and ethylene (80 K at 2.0 mm above the burner surface) [23] flames. The corrected temperature profile of the flame (Fig. 4) was used as an input parameter to predict species mole fraction profiles with the Master Mechanism.

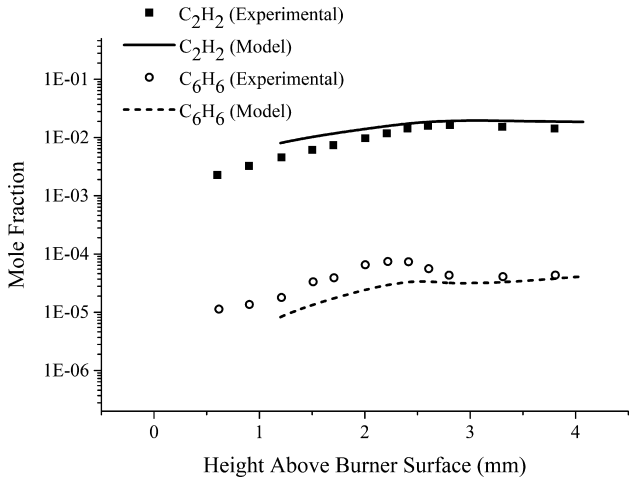

Fig. 2. Validation of the Master Mechanism for mole fractions of C_2H_2 and C_6H_6 in a premixed flame [4].

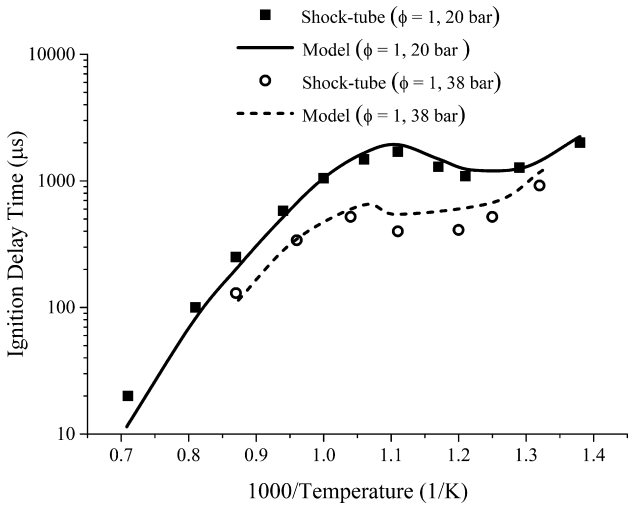

Fig. 3. Validation of the Master Mechanism for ignition delay time in a shock-tube [20].

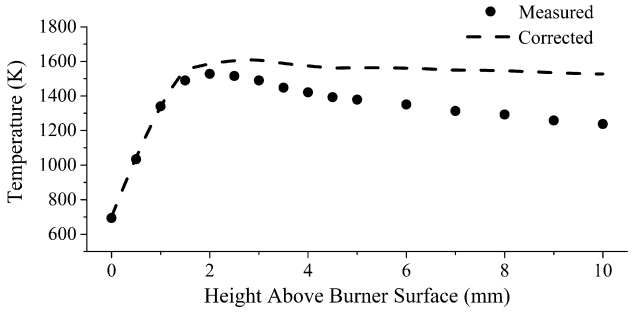

Fig. 4. Measured and corrected temperature profiles of premixed n-heptane flame.

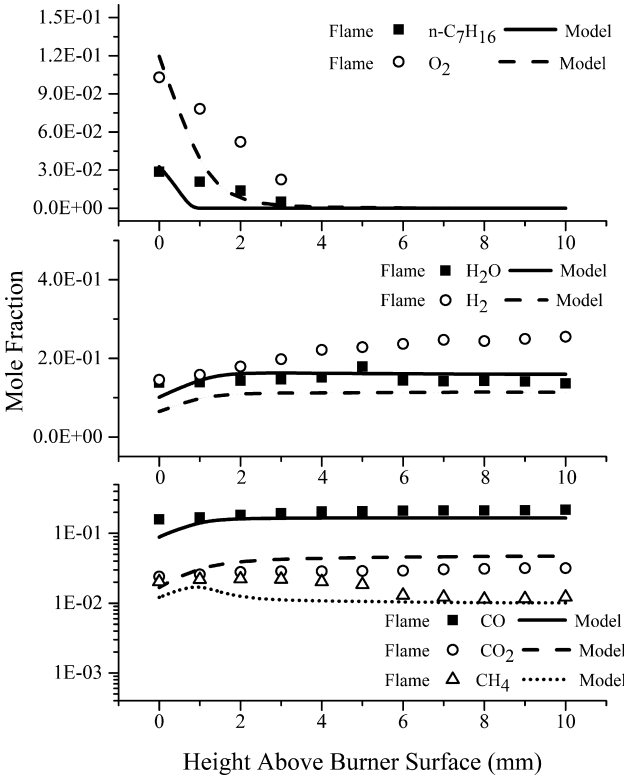

Fig. 5. Comparisons of model predictions with experimental mole fraction profiles for n-C_7H_{16}, O_2, H_2O, H_2, CO, CO_2, and CH_4.

3. Results and discussion

The experimental [8] and model predictions for mole fraction profiles of reactants (O_2 and n-heptane) and low molecular weight products (H_2, H_2O, CO, CO_2, CH_4) are shown in Fig. 5. In the model predictions fuel completely consumed at around 2 mm earlier than the experimental data. For H_2 there was an underestimation by a factor of about 2.5 in the model predictions. A good agreement between experimental measurements and model predictions were achieved for H_2O and C_1 species (CO, CO_2, and CH_4).

The important decomposition routes for n-heptane were investigated by rate of decomposition and reaction pathway analyses. As seen from Fig. 6, all decomposition reactions for n-heptane occurred between burner surface and 1.5 mm HAB. Hydrogen abstraction reactions by H radical from the second and third carbon atoms of n-C_7H_{16} seem to be the most dominant reactions for n-heptane decomposition. Decomposition of n-heptane by hydrogen abstraction with OH radicals started earlier than hydrogen abstraction by H radicals (Fig. 6). At around 0.4 mm HAB, third body reactions that formed C_3 and C_4 alkyls have started. Since all decomposition reactions were in competition at ~0.8 mm HAB, the closest grid point (HAB = 0.8125 mm) was chosen to perform reaction pathway analysis.

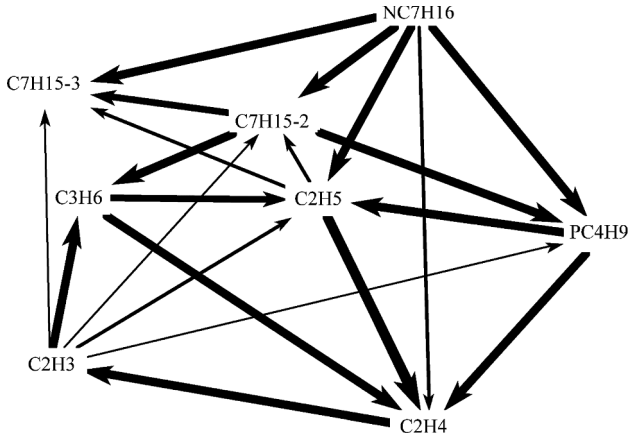

Fig. 7. Main decomposition pathways of n-heptane at HAB = 0.8125 mm (carbon flux).

In Fig. 7, the atomic carbon flux from n-heptane to other species were shown at 0.8125 mm HAB. The formation rates of 3-heptyl (C_7H_{15}-3) and 2-heptyl (C_7H_{15}-2) from n-heptane by H abstraction reactions were analogous to each other (Fig. 7). Additionally, 1-butyl (PC_4H_9). and ethyl (C_2H_5) were directly formed from n-heptane by third body reactions. (2)-heptyl broke down into propene (C_3H_6) and 1-butyl (PC_4H_9). The decomposition path for 3-heptyl was not available in Fig. 7 since decomposition rates of 3-heptyl were very slow compared with those for 2-heptyl at 0.8125 mm HAB.

The measured and predicted mole fraction profiles of C_2 species (C_2H_2, C_2H_4, and C_2H_6), C_3 species (C_3H_4 and C_3H_6), and C_4 species (C_4H_2, C_4H_4, and C_4H_6) are shown in Fig. 8. Among these species, acetylene is an important species that takes a significant role in benzene, PAH and soot formations [17,24,25]. Moreover, propadiene (C_3H_4) and vinylacetylene (C_4H_4) are also considered as precursors for benzene formation [3,26,27]. Vinylacetylene was reported as a

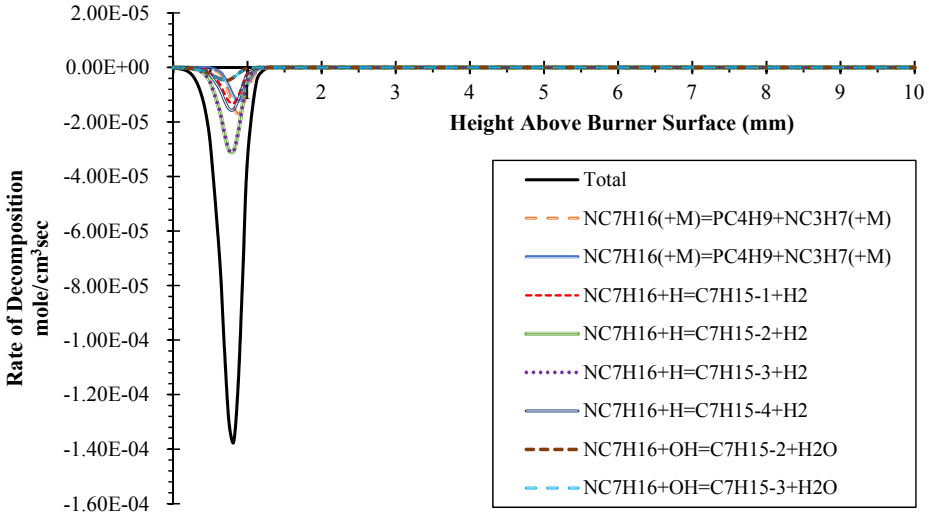

Fig. 6. Rate of production analysis for n-C_7H_{16} across the flame.

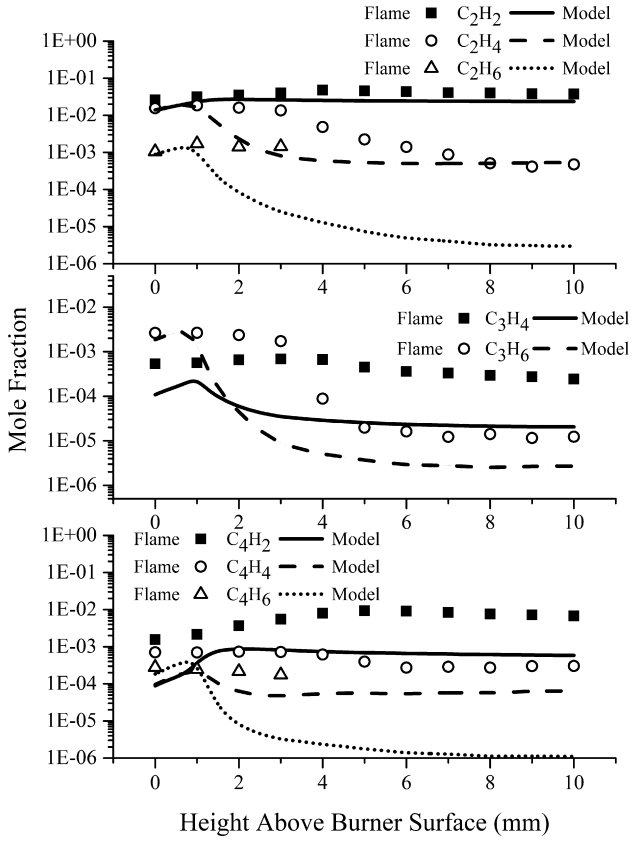

Fig. 8. Comparisons of model predictions with experimental mole fraction profiles for C_2H_2, C_2H_4, C_2H_6, C_3H_4, C_3H_6, C_4H_2, C_4H_4, and C_4H_6.

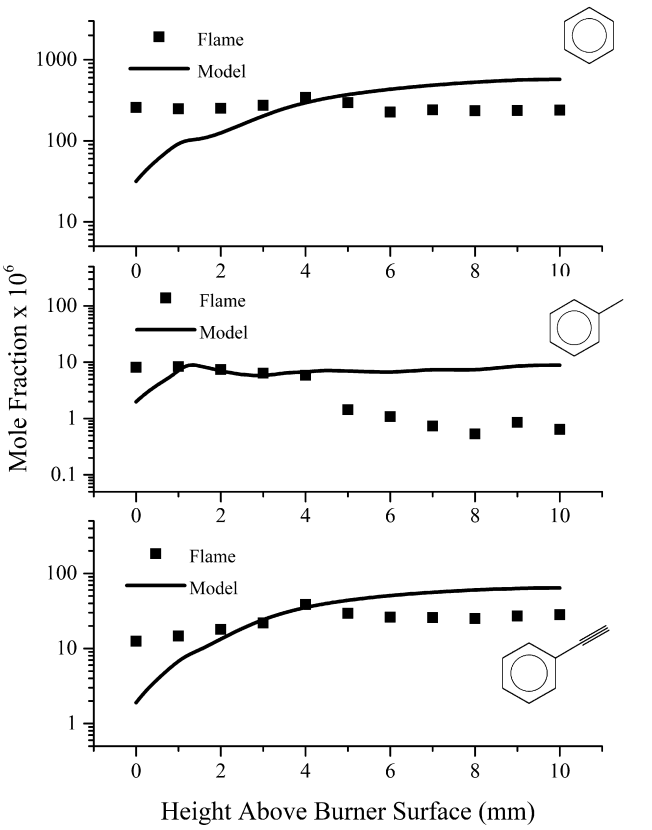

Fig. 9. Comparisons of model predictions with experimental mole fraction profiles for benzene, toluene and phenylacetylene.

precursor for PAH growth [3]. There are other studies in the literature that indicate the importance of propargyl (C_3H_3) and 1,3-butadienyl (1,3-C_4H_5) for benzene formation, and propargyl (C_3H_3) and cyclopentadienyl (C_5H_5) for PAH formation [3]. For these unstable species, there are no experimental data available in the flame studied. The predicted mole fraction profiles of acetylene (C_2H_2) matched with the experimental measurements. However, for ethylene (C_2H_4) mole fraction profile there was a 1.5 mm shift to the burner surface side in the model predictions (Fig. 8). The experimental data for ethane (C_2H_6) were available up to 3 mm HAB. The predicted C_2H_6 mole fractions started to decrease at around 2 mm HAB. The propadiene (C_3H_4) mole fractions were underestimated by the Master Mechanism by a factor of 10 (Fig. 8). For C_3H_6, the model fitted the experimental measurements up to 2 mm HAB, but at higher HAB there were underestimations by the model. The trends for diacetylene (C_4H_2) and vinylacetylene (C_4H_4) mole fraction profiles were successfully computed by the Master Mechanism. However, the mole fractions of both species were underestimated by a factor of about 10 (Fig. 8). In experimental data there were no 1,3-butadiene (C_4H_6) at HAB greater than 3 mm, however, in the model predictions, there was a rapid decrease for C_4H_6 at around 1.5 mm HAB (Fig. 8). In general, there was a good agreement between experimental and modeling results for C_2–C_4 species. Similar differences between modeling results and experimental data were also reported for different flames [9,12].

The experimental data and modeling results for one ring aromatic species benzene (C_6H_6), toluene (C_7H_8), and phenylacetylene (C_8H_6) are shown in Fig. 9. Inal and Senkan [8] have reported that the experimental data for aromatic and PAH species within a few millimeters above the burner surface were questionable due to the possible sampling probe burner surface interactions. Considering their statement, it can be said that both benzene and phenylacetylene mole fractions were slightly overestimated by the Master Mechanism for HAB greater than 4 mm (Fig. 9). However, toluene was overestimated by a factor of about 10 for HAB greater than 4 mm.

It has been reported that 1,3-butadienyl radical (1,3-C_4H_5) was a precursor of benzene in 1,3-butadiene (C_4H_6) flames by the following reaction sequence [24];

$$1,3\text{-}C_4H_5 + C_2H_2 \rightarrow C_6H_7$$

$$C_6H_7 \rightarrow c\text{-}C_6H_7 (\text{ring closure})$$

$$c\text{-}C_6H_7 \rightarrow \text{Benzene} + H (\text{hydrogen loss})$$

The unstable intermediate propargyl (C_3H_3) is also considered as a major precursor for the formation of benzene with the following reaction [18,28];

$$C_3H_3 + C_3H_3 \rightarrow \text{Benzene}$$

The addition of vinyl to vinylacetylene reaction is also regarded as a source of benzene formation especially in ethylene flames [28];

$$C_4H_4 + C_2H_3 \leftrightarrow C_6H_6 + H$$

To see the important reactions for the formation of benzene in the fuel-rich n-heptane flame, rate of production analysis for benzene across the flame was carried out. The most significant eight reactions on the formation and decomposition of benzene can be seen in Fig. 10. The maximum benzene production was achieved at around 1.25 mm HAB. Between 1.4 mm and 2.4 mm HAB, benzene decomposition was faster than its production. The most effective reaction for benzene destruction and formation seems to be hydrogen abstraction reaction from benzene. Combination of propargyl (C_3H_3) reactions also led to benzene formation especially at HAB of ~ 2 mm. The forward reaction between toluene and H ($C_6H_5CH_3 + H = A_1 + CH_3$) also resulted to benzene formation. Since the maximum total ROP of benzene was at around 1.25 mm HAB, the reaction pathway analysis for benzene was performed at that height.

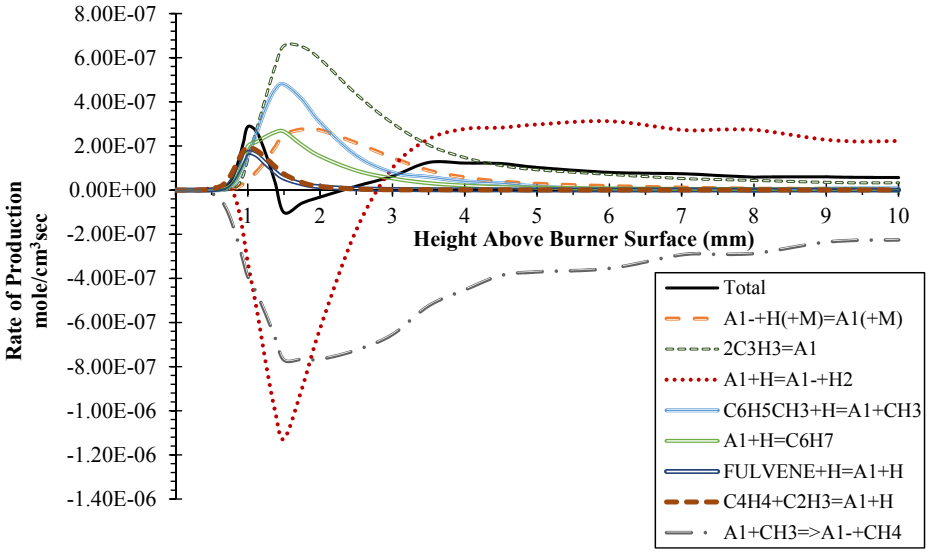

Fig. 10. Rate of production analysis for benzene across the flame.

The simplified formation pathways of benzene (in both C and H fluxes) are shown in Fig. 11. Bimolecular reaction between two propargyl radicals (C_3H_3) was found as the most dominant route for benzene formation. Vinyl (C_2H_3) addition to vinylacetylene (C_4H_4) reaction also produced a comparable amount of benzene. However, the reactions between propadiene (C_3H_4-A) and propargyl radical and acetylene addition to 1,3-butadienyl radical (1,3-C_4H_5) were found to be less important in benzene formation under the conditions considered.

Two membered PAH naphthalene is also considered as an alternative first aromatic ring in hydrocarbon combustion and pyrolysis by the following reaction [3,29],

$$C_5H_5 + C_5H_5 \leftrightarrow A_2 + H + H$$

where A_2 refers to naphthalene. It is also suggested that phenylacetylene can be formed as a first aromatic ring by the reaction $C_4H_4 + C_4H_4(+H)$ [30].

Hydrogen abstraction acetylene addition (HACA) is one of the main reaction mechanism that results in PAH formation [2,25]. That mechanism relied on the addition of acetylene to phenyl (for i = 1) radical to grow their molecule and after the necessary amount of carbon is achieved two or more membered aromatic species can be formed;

$$A_i + H \leftrightarrow A_{i-} + H_2$$

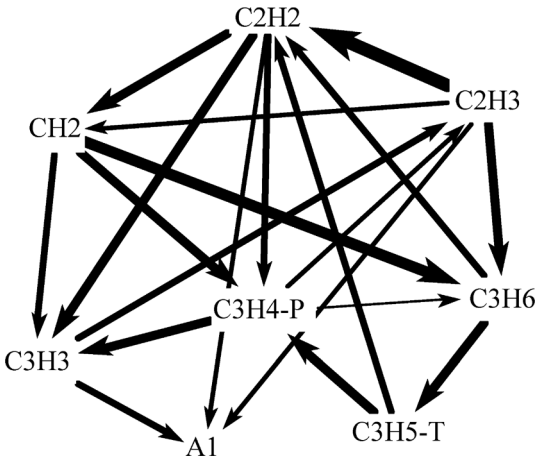

Fig. 11. Main formation pathways of benzene (A1) at HAB = 1.25 mm (both carbon and hydrogen fluxes).

$$A_{i-} + C_2H_2 \leftrightarrow A_iC_2H_2$$

$$A_iC_2H_2 + C_2H_2 \leftrightarrow A_{i+1} + H$$

Vinylacetylene addition to aromatic radical and fusion of aromatic radical with an aromatic ring also considered as growth mechanism of polycyclic aromatic hydrocarbons [25];

$$A_i + C_4H_4 \leftrightarrow A_iC_4H_4 \rightarrow A_{i+1}$$

$$A_{1-} + A_1 \rightarrow P_2$$

where P_2 is biphenyl and A_i is PAH with i number of benzene ring.

Hydrogen abstraction methyl addition (HAMA) sequence was also considered as an alternative reaction sequence for PAH growth [31].

The experimental measurements and modeling results for the mole fraction profiles of indene, naphthalene, and acenaphthylene are shown in Fig. 12. For indene, the model underpredicted the experimental data by a factor of about 10 up to 5 mm HAB while the difference between model predictions and the experimental data was about a factor of 3 for HAB above 6 mm (Fig. 12). Naphthalene was underpredicted by the model up to 5 mm HAB. However, the model predictions of naphthalene became very close to experimental data for HAB greater than 6 mm. Acenaphthylene was underpredicted by the model up to 2 mm HAB. However, for HAB greater than 2 mm the model predictions were very close to the experimental data.

For three ring PAH species phenanthrene, anthracene and 4H-cyclopenta[def]phenanthrene, experimental data and model predictions for mole fraction profiles are shown in Fig. 13. The Master Mechanism was able to predict both phenanthrene and anthracene concentration profiles with an error less than a factor of 3 especially at higher distances above the burner surface (Fig. 13). The model underpredicted the 4H-cyclopenta[def]phenanthrene mole fractions by a factor of 10 when compared with the experimental data (Fig. 13).

Fluoranthene and pyrene experimental mole fraction profiles with model predictions are presented in Fig. 14. The experimental fluoranthene mole fractions and modeling results match with each other. Pyrene mole fractions were underestimated by the Master Mechanism about a factor of 5 for HAB greater than 5 mm. The difference between experimental data and the model predictions of PAHs can be considered acceptable. There was more than a factor of 100 difference between experimental data and model predictions for pyrene and phenanthrene mole fractions in a fuel-rich, premixed ethylene flame [32].

There are several methods suggested in the literature to apply mechanism reduction, such as principal component analysis, directed relation graph method (DRG) [33], directed relation graph with error

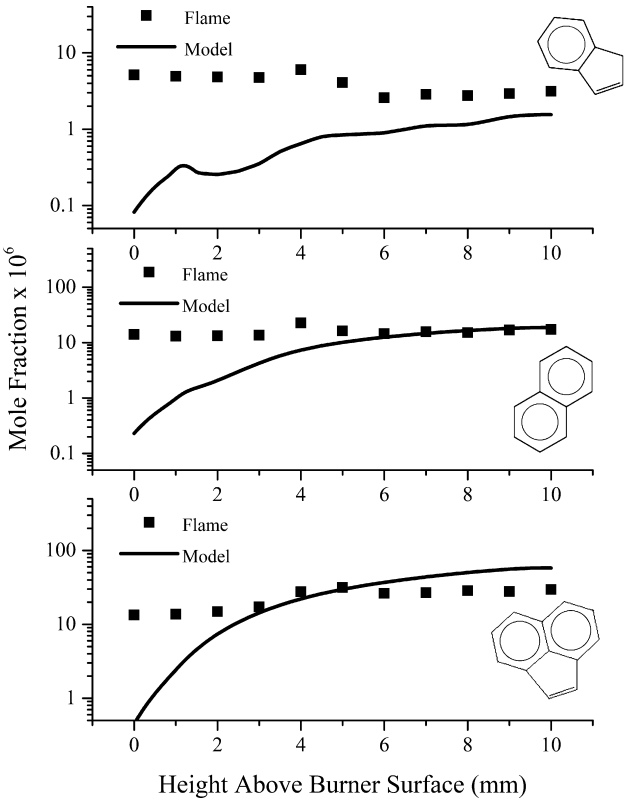

Fig. 12. Comparisons of model predictions with experimental mole fraction profiles for indene, naphthalene, and acenaphthylene.

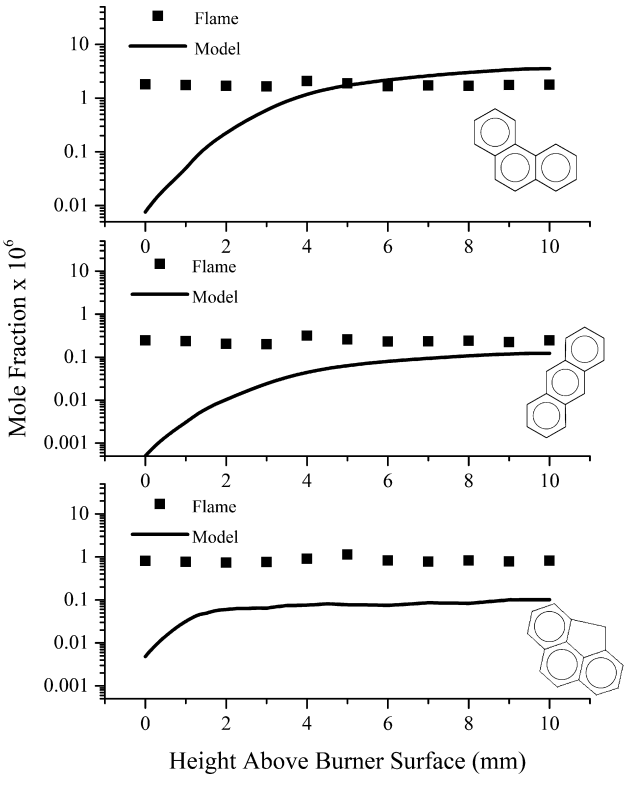

Fig. 13. Comparisons of model predictions with experimental mole fraction profiles for phenanthrene, anthracene, and 4H-cyclopenta[def]phenanthrene.

production (DRGEP) [34], directed relation graph method with path flux analysis (DRGPFA) [35], and isomer lumping. In this study, directed relation graph with error propagation method was used to obtain

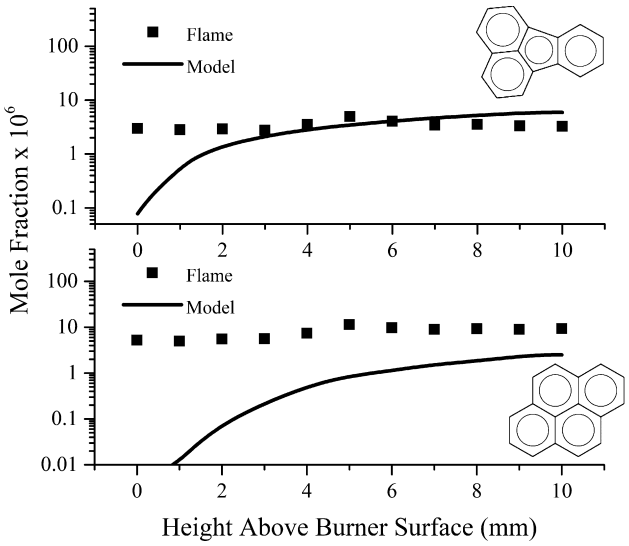

Fig. 14. Comparisons of model predictions with experimental mole fraction profiles for fluoranthene and pyrene.

a Skeletal or Reduced Mechanism from the Master Mechanism.

In DRG method, the removal of a species on the production rate of selected species was defined as an immediate error, (r_{AB}) where A is the selected species and B is the removed species. The immediate error is calculated by the equation below [33],

$$r_{AB} \equiv \frac{\sum_{i=1,j} |\nu_{A,i}\omega_i \delta_{Bi}|}{\sum_{i=1,j} |\nu_{A,i}\omega_i|} \tag{3}$$

$$\delta_{Bi} = \begin{bmatrix} 1, & \text{if the i}^{\text{th}}\text{ reaction involves species B} \\ 0, & \text{otherwise} \end{bmatrix}$$

where i is the reaction number, $\nu_{A,i}$ the stoichiometric coefficient of species A in the i^{th} reaction, and ω_i the reaction rate of the i^{th} reaction. Denominator includes all the reactions in the mechanism, however, the numerator just includes the reactions that consist of species B. If the calculated immediate error is greater than the error-tolerance level, the specie would not be eliminated.

In DRGEP method an additional R-value is defined to determine the species required to be kept in the mechanism. The R-value is defined as [34];

$$R_A(B) = max_S\{r_{ij}\} \tag{4}$$

where S is the group of all possible paths from species A to species B, and r_{ij} the immediate error. For the reaction sequence of A → B → C, the R value is $r_{AB} \times r_{BC}$. If there is a reaction between A and B with a larger R value than the threshold value, species B needs to be kept in the mechanism.

As the relative tolerance increases, the number of eliminated reactions also increase. To start mechanism reduction, the relative tolerance of all the major, minor, and trace species that experimentally quantified were defined. By defining the relative tolerance as a high value, it was possible to see different versions of reduced mechanisms.

Reduced mechanisms that have different number of species/reactions with their error percentages of n-heptane mole fractions are shown in Fig. 15. The error percentage was related to the difference between n-heptane mole fractions in the Master and Reduced Mechanisms. The threshold values are related with the removal of the species/reactions. Threshold value of 1 means the removal of all species/reactions. There were two sudden increases in the percentage error of n-heptane mole fraction predictions with the increasing threshold value. The reduced mechanism which corresponds to a threshold value of 0.111 was chosen as the best Skeletal or Reduced Mechanism

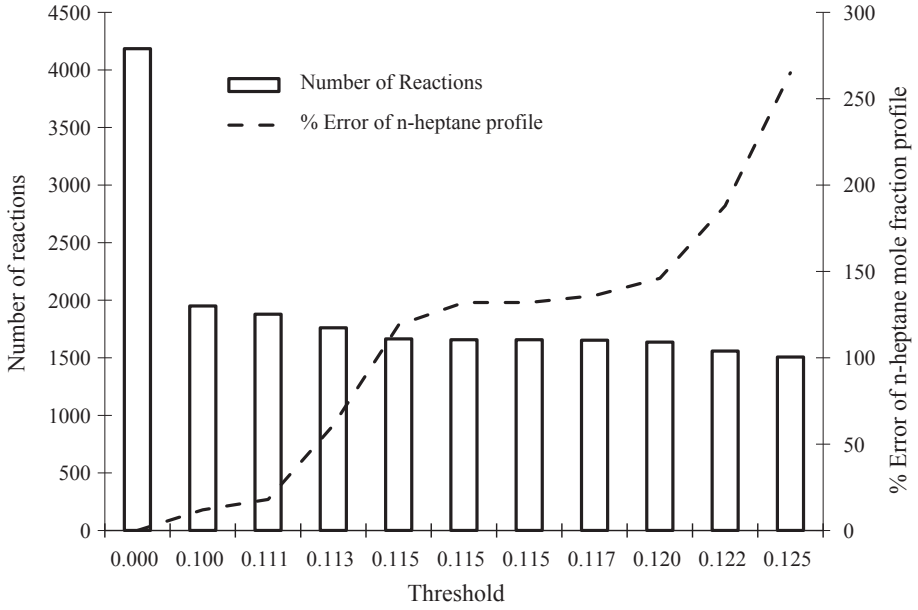

Fig. 15. Effects of threshold value on number of reactions and percentage error of n-heptane mole fraction predictions in the reduced mechanism.

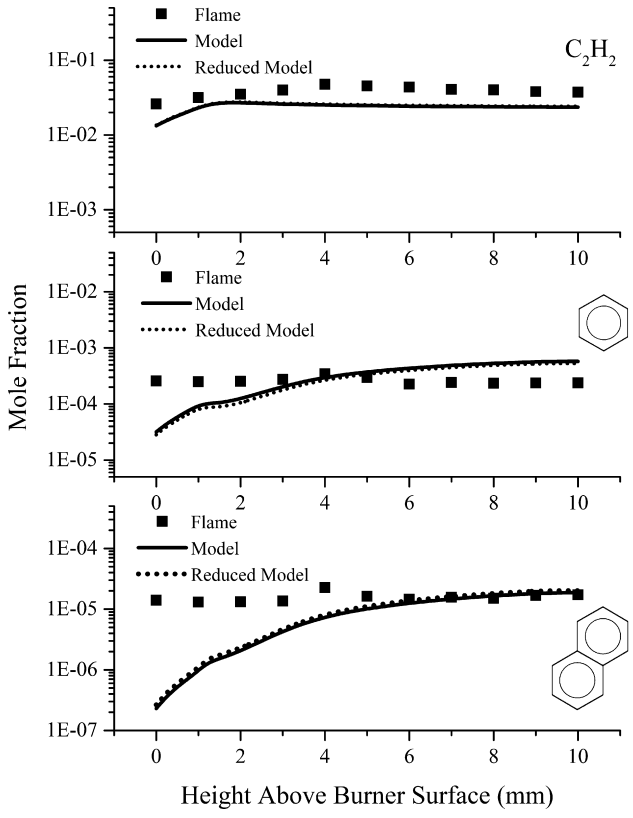

Fig. 16. Comparisons of detailed and reduced model predictions with experimental mole fraction profiles for acetylene, benzene, and naphthalene.

(Fig. 15). As a result of mechanism reduction, a Skeletal Mechanism with 1879 reactions and 359 species was achieved.

Fig. 16 shows the experimental mole fractions of acetylene, benzene, and naphthalene with the Master and Skeletal Mechanism predictions. As seen from Fig. 16, the performances of the Skeletal and Master Mechanisms were almost the same for the species considered in the fuel-rich n-heptane flame.

4. Conclusion

A burner-stabilized, premixed, laminar, fuel-rich n-heptane flame at an equivalence ratio of 2.10 was modeled using DCKM approach. A detailed chemical kinetic mechanism was generated by merging Base and Donor Mechanisms. The Base Mechanism was about the detailed oxidation pathways of n-heptane in a wide range of conditions. Donor Mechanisms include the formation pathways of benzene and polycyclic aromatic hydrocarbons. Some reaction rate parameters were also modified to improve the model predictions over the experimental data. The resulting Master Mechanism consists of 4185 reactions and 893 species. It was validated by experimental data of species mole fractions in jet stirred reactors (JSRs) and premixed flame, and ignition delay time measurements in shock-tube. The Master Mechanism was able to predict most of the major, minor, and trace species mole fractions of the premixed, fuel-rich, n-heptane flame. By the rate of production and reaction pathway analyses, it was seen that propargyl radical (C_3H_3), vinylacetylene (C_4H_4), and acetylene (C_2H_2) were the main precursors for the formation of benzene. The Skeletal Mechanism was generated by the directed relation graph with error propagation method. It consists of 1879 reactions and 359 species. The Skeletal Mechanism was in a good agreement with the Master Mechanism on the species mole fraction predictions of the n-heptane flame. It can be used to simulate complex combustion processes without compromising the descriptive ability of the Master Mechanism.

Declaration of Competing Interest

The authors declare that they have no known competing financial interests or personal relationships that could have appeared to influence the work reported in this paper.

Acknowledgement

We would like to thank Izmir Institute of Technology Scientific Research Fund (Project Number: 2017IYTE41) for the financial support.

References

[1] Larsen JC. Polyaromatic hydrocarbons (PAH). Evaluation of Health Hazards and Estimation of A Quality Criterion in Soil. National Food Institute, Technical

University of Denmark; 2013. p. 24.
[2] Frenklach M, Wang H. Detailed modeling of soot particle nucleation and growth. Proc Combust Inst 1991;23(1):1559–66.
[3] Richter H, Howard JB. Formation of polycyclic aromatic hydrocarbons and their growth to soot—a review of chemical reaction pathways. Prog Energy Combust Sci 2000;26(4):565–608.
[4] Bakali AE, Delfau JL, Vovelle C. Experimental study of 1 atmosphere, rich, premixed n-heptane and iso-octane flames. Combust Sci Technol 1998;140(1–6):69–91.
[5] Doute C, Delfau JL, Akrich R, Vovelle C. Experimental study of the chemical structure of low-pressure premixed n-heptane-O2-Ar and iso-octane-O2-Ar flames. Combust Sci Technol 1997;124(1–6):249–76.
[6] Chaos M, Kazakov A, Zhao Z, Dryer FL. A high-temperature chemical kinetic model for primary reference fuels. Int J Chem Kinet 2007;39(7):399–414.
[7] Marchal C, Delfau J-L, Vovelle C, Moréac G, Mounaïm-Rousselle C, Mauss F. Modelling of aromatics and soot formation from large fuel molecules. Proc Combust Inst 2009;32(1):753–9.
[8] Inal F, Senkan SM. Effects of equivalence ratio on species and soot concentrations in premixed n-heptane flames. Combust Flame 2002;131(1):16–28.
[9] Raj A, Prada IDC, Amer AA, Chung SH. A reaction mechanism for gasoline surrogate fuels for large polycyclic aromatic hydrocarbons. Combust Flame 2012;159(2):500–15.
[10] Wang H, Yao M, Yue Z, Jia M, Reitz RD. A reduced toluene reference fuel chemical kinetic mechanism for combustion and polycyclic-aromatic hydrocarbon predictions. Combust Flame 2015;162(6):2390–404.
[11] Park S, Wang Y, Chung SH, Sarathy SM. Compositional effects on PAH and soot formation in counterflow diffusion flames of gasoline surrogate fuels. Combust Flame 2017;178(Supplement C):46–60.
[12] Seidel L, Moshammer K, Wang X, Zeuch T, Kohse-Höinghaus K, Mauss F. Comprehensive kinetic modeling and experimental study of a fuel-rich, premixed n-heptane flame. Combust Flame 2015;162(5):2045–58.
[13] An Y-z, Pei Y-q, Qin J, Zhao H, Li X. Kinetic modeling of polycyclic aromatic hydrocarbons formation process for gasoline surrogate fuels. Energy Convers Manage 2015;100(Supplement C):249–61.
[14] Mehl M, Pitz WJ, Westbrook CK, Curran HJ. Kinetic modeling of gasoline surrogate components and mixtures under engine conditions. Proc Combust Inst 2011;33(1):193–200.
[15] ANSYS Chemkin-Pro®. Chemkin (19.0). Release 19.0 ed.: ANSYS, Inc.; 2018-01-11.
[16] Hakka HM, Cracknell RF, Pekalski A, Glaude PA, Battin-Leclerc F. Experimental and modeling study of ultra-rich oxidation of n-heptane. Fuel 2015;144(Supplement C):358–68.
[17] Wang H, Frenklach M. A detailed kinetic modeling study of aromatics formation in laminar premixed acetylene and ethylene flames. Combust Flame 1997;110(1–2):173–221.
[18] Marinov NM, Pitz WJ, Westbrook CK, Vincitore AM, Castaldi MJ, Senkan SM, et al. Aromatic and polycyclic aromatic hydrocarbon formation in a laminar premixed n-butane flame. Combust Flame 1998;114(1):192–213.
[19] Richter H, Benish TG, Mazyar OA, Green WH, Howard JB. Formation of polycyclic aromatic hydrocarbons and their radicals in a nearly sooting premixed benzene flame. Proc Combust Inst 2000;28(2):2609–18.
[20] Zhang K, Banyon C, Bugler J, Curran HJ, Rodriguez A, Herbinet O, et al. An updated experimental and kinetic modeling study of n-heptane oxidation. Combust Flame 2016;172:116–35.
[21] Tsang W, Hampson R. Chemical kinetic data base for combustion chemistry. Part I. Methane and related compounds. J Phys Chem Ref Data 1986;15(3):1087–279.
[22] McEnally CS, Köylü ÜÖ, Pfefferle LD, Rosner DE. Soot volume fraction and temperature measurements in laminar nonpremixed flames using thermocouples. Combust Flame 1997;109(4):701–20.
[23] Castaldi MJ, Marinov NM, Melius CF, Huang J, Senkan SM, Pit WJ, et al. Experimental and modeling investigation of aromatic and polycyclic aromatic hydrocarbon formation in a premixed ethylene flame. Proc Combust Inst 1996;26(1):693–702.
[24] Cole JA, Bittner JD, Longwell JP, Howard JB. Formation mechanisms of aromatic compounds in aliphatic flames. Combust Flame 1984;56(1):51–70.
[25] Appel J, Bockhorn H, Frenklach M. Kinetic modeling of soot formation with detailed chemistry and physics: Laminar premixed flames of C2 hydrocarbons. Combust Flame 2000;121(1):122–36.
[26] Wu CH, Kern RD. Shock-tube study of allene pyrolysis. J Phys Chem 1987;91(24):6291–6.
[27] Mebel AM, Lin SH, Yang XM, Lee YT. Theoretical study on the mechanism of the dissociation of benzene. The C5H3 + CH3 product channel. J Phys Chem A 1997;101(36):6781–9.
[28] Richter H, Howard JB. Formation and consumption of single-ring aromatic hydrocarbons and their precursors in premixed acetylene, ethylene and benzene flames. Phys Chem Chem Phys 2002;4(11):2038–55.
[29] Ikeda E, Tranter RS, Kiefer JH, Kern RD, Singh HJ, Zhang Q. The pyrolysis of methylcyclopentadiene: Isomerization and formation of aromatics. Proc Combust Inst 2000;28(2):1725–32.
[30] Lin H, Liu P, He Z, Zhang Y, Guan B, Huang Z. Formation of the first aromatic ring through the self-recombination of but-1-ene-3-yne with H-assistance in combustion. Int J Hydrogen Energy 2016;41(31):13736–46.
[31] Hansen N, Schenk M, Moshammer K, Kohse-Höinghaus K. Investigating repetitive reaction pathways for the formation of polycyclic aromatic hydrocarbons in combustion processes. Combust Flame 2017;180:250–61.
[32] Liu P, Li Z, Bennett A, Lin H, Sarathy SM, Roberts WL. The site effect on PAHs formation in HACA-based mass growth process. Combust Flame 2019;199:54–68.
[33] Lu T, Law CK. A directed relation graph method for mechanism reduction. Proc Combust Inst 2005;30(1):1333–41.
[34] Pepiot-Desjardins P, Pitsch H. An efficient error-propagation-based reduction method for large chemical kinetic mechanisms. Combust Flame 2008;154(1):67–81.
[35] Sun W, Chen Z, Gou X, Ju Y. A path flux analysis method for the reduction of detailed chemical kinetic mechanisms. Combust Flame 2010;157(7):1298–307.